



Contents lists available at ScienceDirect

Journal of Orthopaedic Translation

journal homepage: www.journals.elsevier.com/journal-of-orthopaedic-translationFavorable osteogenic activity of iron doped in silicocarnotite bioceramic: In vitro and *in vivo* StudiesJingwei Zhang^{a,1}, Fanyan Deng^{c,1}, Xiaoliang Liu^{a,1}, Yuwei Ge^d, Yiming Zeng^a, Zanjing Zhai^a, Congqin Ning^{b,**}, Huiwu Li^{a,*}^a Shanghai Key Laboratory of Orthopaedic Implants, Department of Orthopaedic Surgery, Shanghai Ninth People's Hospital, Shanghai Jiaotong University School of Medicine, 639# Zhizaoju Road, Shanghai, 200011, PR China^b The Education Ministry Key Lab of Resource Chemistry and Shanghai Key Laboratory of Rare Earth Functional Materials, Shanghai Normal University, 100# Guilin Road, Shanghai, 200234, China^c State Key Laboratory of High Performance Ceramics and Superfine Microstructure, Institute of Ceramics, Chinese Academy of Sciences, 1295# Dingxi Road, Shanghai, 200050, China^d Department of Orthopedic Surgery, Shanghai Jiao Tong University Affiliated Sixth People's Hospital, 600# Yishan Road, Shanghai, 200233, China

ARTICLE INFO

Keywords:

Bioceramic
Bone formation
Iron
Osteogenic activity
Silicocarnotite

ABSTRACT

Background: Calcium phosphate silicate (Ca₅(PO₄)₂SiO₄ or CPS) is a promising bioceramic for bone grafting. Iron (Fe) is a trace element in the human body that has been reported to enhance the mechanical strength of CPS ceramics. However, the exact biofunctions of Fe, combined with another human trace element, viz. silicon (Si), in CPS and the optimal dose for Fe addition must be further investigated.**Methods:** *In vitro*: the morphology, structure and cell adhesion were observed by SEM; the ability to promote osteogenic differentiation and mineralization was explored by ALP and alizarin red staining; the expression of osteogenic-specific genes and proteins was detected by PCR, WB and immunofluorescence. *In vivo*: Further exploration of bone regeneration capacity by establishing a skull defect model.**Results:** *In vitro*, we observed increased content of adhesion-related proteins and osteogenic-related genes expression of Fe-CPS compared with CPS, as demonstrated by immunofluorescence and polymerase chain reaction experiments, respectively. *In vivo* micro-computed tomography images, histomorphology, and undecalcified bone slicing also showed improved osteogenic ability of Fe-CPS bioceramics.**Conclusion:** With the addition of Fe₂O₃, the new bone formation rate of the Fe-CPS scaffold after 12 weeks increased from 9.42% to 43.76%. Moreover, both *in vitro* and *in vivo* experimental outcomes indicated that Fe addition improved the CPS bioceramics in terms of their osteogenic ability by promoting the expression of osteogenic-related genes. Fe-CPS bioceramics can be employed as a novel material for bone tissue engineering on account of their outstanding new bone formation ability.**The translational potential of this article:** This study suggests that Fe-CPS bioceramics can be employed as a novel material for bone tissue engineering on account of their outstanding new bone formation ability, which provides promising therapeutic implants and strategies for the treatment of large segmental bone defects.

1. Introduction

Bone defects arising from tumors, infections, trauma, and other bone diseases constitute one of the most difficult problems in orthopaedics [1–3] and can interfere with process of the formation of new bones.

Improving new bone formation in patients with bone defects is therefore one of the major challenges faced by orthopedic surgeons. In response, a large variety of bone grafts, for instance, allografts, autografts and xenografts, have been proposed, that can substantially increase bone formation and improve clinical outcomes [4]. However, these bone grafts

* Corresponding author.

** Corresponding author.

E-mail addresses: zjw_ys@163.com (J. Zhang), dengfanyan@mail.sic.ac.cn (F. Deng), Abel.liuxl@outlook.com (X. Liu), geyw2000@163.com (Y. Ge), xyhz29@163.com (Y. Zeng), zanjing_zhai@163.com (Z. Zhai), cqning@mail.sic.ac.cn (C. Ning), huiwu1223@163.com (H. Li).¹ Both authors equally contributed to this work.<https://doi.org/10.1016/j.jot.2021.12.002>

Received 15 August 2021; Received in revised form 6 December 2021; Accepted 7 December 2021

have certain disadvantages, such as donor-site morbidity, difficulty in obtaining autografts, and disease spread and rejection in allografts and xenografts [5–9]. Tissue engineering is a novel method for overcoming the limitations associated with bone grafts and for improving the healing process in bone defects, with artificial bone repair biomaterials currently receiving increasing attention [8].

Calcium phosphate silicate ($\text{Ca}_5(\text{PO}_4)_2\text{SiO}_4$, CPS) is a novel bioceramic [10] that has been widely recognized as a promising bone graft biomaterial, given its good cytocompatibility and potentially good osteogenic activity, as revealed by *in vitro* experiments [10,11]. Owing to the presence of Si, which has a positive influence on bone formation [12,13], CPS shows better apatite formation ability and bone formation ability than calcium phosphate bioceramics. However, the mechanical properties and osteoinductivity of CPS bioceramics, along with cytocompatibility and osteoconductivity, which are critical properties of artificial bone repair materials [14,15], need to be improved further. Previously employed biomaterials, such as hydroxyapatite, tricalcium phosphate (TCP), and calcium phosphate cement, have proven to have sufficient biocompatibility and acceptable osteoconductivity, but lack osteoinductivity [16–18]. Improving biomaterial osteoinductivity and bioactivity is a major challenge associated with the development of artificial bone repair biomaterials.

One solution to the above-mentioned problems is to add trace elements, such as Zn, Mg, Fe, Mn, and Sr, with several articles reporting their use in tricalcium phosphate scaffolds and calcium phosphate [18–22]. Iron (Fe) is one of the most abundant fundamental trace elements in humans, especially in bone tissues [23]. As one of the important trace elements present naturally in bones, Fe plays a vital role in bone metabolism [23,24]. Bio-iron is an indispensable constituent of enzymes and cytochromes and regulates various physiological processes simultaneously [23]. It has been reported that the bone density of mice increases with increasing Fe content in the breeding environment [25,26]; when the intake of Fe-containing food is reduced, the bone density decreases, and the bone fragility increases, which can easily lead to osteoporosis. It has also been found that insufficient Fe intake affects the differentiation and mineralization of osteoblasts, and the prerequisite for its mineralization must be the synthesis of collagen fibers [25,27]. As has been previously reported, Fe can affect collagen synthesis and vitamin D metabolism [28], while abnormal iron concentrations can affect osteoblast activity and cause abnormal bone metabolism [23,29]. Therefore, it is speculated that Fe affects bone regeneration by affecting the synthesis of collagen fibers.

A previous study conducted by our team showed that Fe could improve CPS ceramics in terms of their mechanical strength and preserve the excellent capability of apatite formation simultaneously [30]. It has recently been reported that appropriate amounts of Fe added to biomaterials are safe and promote biomaterial bioactivity [18,31–33]. A correlation study showed that adding Fe to TCP can promote osteoblast proliferation and differentiation in an *in vitro* test [18]. Therefore, Fe is a promising element that is expected to improve the osteoinductivity of artificial bone repair biomaterials. However, the exact biofunction of Fe when added to the CPS remains unclear. Another important factor governing the behavior of biomaterials is the content of Fe added, both *in vitro* and *in vivo*. A small number of studies have also shown that excess Fe can cause cytotoxicity [29,33]. Excessive amounts of Fe can adversely affect the biological properties of materials [23,29,33]. Determining the appropriate Fe content is therefore a crucial problem that must be solved when modifying this specific ceramic. Therefore, the exact biofunction and the appropriate content of iron ions added to CPS require further investigation.

In this study, we studied Fe-CPS bioceramics to improve biocompatibility by the formation of adhesion proteins to simultaneously promote the ability of new bone formation by the released iron ions. This study speculates that iron ions can be released slowly from Fe-CPS, and the released ions enter osteoblasts to promote the formation of adhesion proteins and osteoblast differentiation. Thus, the increased adhesion of

osteoblasts to the Fe-CPS surface and promoted osteoblast differentiation resulted in enhanced bone regeneration.

2. Methods

2.1. Preparing the Fe-CPS scaffolds

To prepare the Fe-CPS bioceramics, the sol–gel method was used to fabricate the CPS powders, and the specific process was described in another article [30]. Briefly, tetraethyl orthosilicate (TEOS; $\text{Si}(\text{OC}_2\text{H}_5)_4$, AR, Sinopharm Chemical Reagent Co., Ltd., Shanghai, China), triethyl phosphate (TEP; $\text{OP}(\text{C}_2\text{H}_5\text{O})_3$, CP, Sinopharm Chemical Reagent Co., Ltd., Shanghai, China), and $\text{Ca}(\text{NO}_3)_2 \cdot 4\text{H}_2\text{O}$ (AR, Sinopharm Chemical Reagent Co., Ltd., Shanghai, China) were hydrolyzed in a solution of deionized water and ethanol ($V_{\text{Water}}:V_{\text{EtOH}} = 3:1$) in sequence, and 2 N HNO_3 was used as the catalyst. After aging and drying, the obtained powders were calcined for 6 h at 1350 °C to achieve CPS. Fe_2O_3 (AR, Sinopharm Chemical Reagent Co., Ltd., Shanghai, China) was employed as an additive to prepare 0, 0.5, 1, and 1.5 wt% Fe_2O_3 -CPS solutions (indicated as CPS, 0.5Fe-CPS, 1Fe-CPS, and 1.5Fe-CPS, respectively) using a mechanical mixing method, and 1 wt% polyvinyl alcohol (PVA) as a binder. To reduce the impact of different porosities on the biological attributes of bioceramics based on Fe-CPS *in vitro* and *in vivo*, 40–65 wt% polyethylene glycol (PEG) particles of size 150–300 μm was added as pore formers to produce porous Fe-CPS bioceramics, and the porosity of all scaffolds was ~65%, as estimated by the Archimedes method. All the Fe-CPS scaffolds were heated for 2 h at 500 °C, with a heating rate of 2 °C/min to exhaust the PEG and later sintered for 2 h at 1300 °C at a heating rate of 5 °C/min.

2.2. Characterizing the Fe-CPS scaffolds

The composition of the Fe-CPS bioceramics was investigated through X-ray diffraction (XRD, D/MAX-RBX, Rigaku, Japan) analysis in the 2 θ range of 10°–60° employing a step size of 5°/min. To observe the morphology of the Fe-CPS porous scaffolds, we employed a tungsten filament scanning electron microscope (SEM, S-3400 N Type I, HITACHI, Japan).

2.3. Extract preparation of Fe-CPS bioceramics

To investigate the element concentration of the Fe-CPS bioceramics, we immersed all the samples in 5.0 mL basic minimum essential medium alpha (MEM- α ; Gibco, Invitrogen, Inc.). The medium (1.0 mL) was extracted and the same volume of MEM- α was added at a specified time point. The ISO 10993-5 standard was followed while prepare the extracts. The mass-to-extraction-medium ratio was 0.2 g/mL, and the immersed samples were kept at 37 °C for 24 h in a moisturized ambient with 5% CO_2 . We determined the calcium, phosphorus, Si, and Fe concentrations using inductively coupled plasma atomic emission spectroscopy (Vista AXE, Varian, Palo Alto, CA).

2.4. Cell culture and viability

The Shanghai Institutes for Biological Science, Chinese Academy of Science (Shanghai, China) provided cells from the osteoblastic cell line MC3T3-E1. Shanghai Rothen Biotechnology Co(Shanghai, China) provided human bone marrow mesenchymal stem cells (hBMSCs). An animal hospital affiliated with Shanghai Jiao Tong University signed the approval document. The hBMSCs were grown in a medium comprising 1% penicillin/streptomycin and 10% foetal calf serum in 5% CO_2 at 37 °C. For cell viability assays, we planted 1×10^4 MC3T3-E1 cells in the plates containing 96 wells and incubated them for 24 h. As a cultivation milieu, we used CPS or Fe-CPS bioceramic extract. After culturing for 1, 2, and 3 days in the extracted CPS or Fe-CPS bioceramic solutions, cytotoxicity was assessed employing the Cell Counting Kit-8 (CCK-8,

Dojindo, Kumamoto, Japan).

2.5. Alkaline phosphatase activity and alizarin staining

hBMSCs were seeded in the plates containing 24 wells for 24 h. Extraction of the CPS or Fe-CPS bioceramic was used as the culture medium. Following the cultivation for 7 days, the hBMSCs were fixed with 4% paraformaldehyde, rinsed twice with phosphate-buffered saline, and then stained with an alkaline phosphatase (ALP) kit or alizarin (Hongqiao, Shanghai, China). Subsequently, we detected hBMSCs using optical microscopy.

2.6. Quantitative polymerase chain reaction for ALP, osteopontin, and runt-related transcription factor 2

We seeded and cultured 4×10^6 MC3T3-E1 cells/well in 24-well plates using the extracted CPS and Fe-CPS bioceramic solutions. After culturing the plates for 5 days, total RNA was collected employing the RNeasy Mini kit (Qiagen, Valencia, CA, USA), which was then synthesized into cDNA through reverse transcriptase (TaKaRa). We employed SYBR1 Premix ExTaq™ II (TaKaRa) and an ABI 7500 Sequencing Detection System (Applied Biosystems, Foster City, CA, USA) in real-time polymerase chain reaction (RT-PCR). The PCR primers were designed as given below:

Runx2 forward 5'-GACTGTGGTTACCGTCATGGC-3'.
and reverse 5'-ACTTGGTTTTTCATAACAGCGGA-3'.
ALP forward 5'-AGAAGTTCGCTATCTGCCTTGCT-3'.
and reverse 5'-TGGCCAAAGGGCAATAACTAGGGA-3'.
OPN forward 5'-ACCCAGATCCTATAGCCACATG-3'.
and reverse 5'-TGGAATTGCTTGGGAAGAGTTTC-3'.

2.7. Cell adhesion

For the immunofluorescence of the adhesion-related proteins, Rho-protein, vinculin, and myosin, hBMSCs were seeded into the plates containing 24 wells (1×10^4 cells/well) and co-cultured them with CPS or Fe-CPS bioceramics for 12 h. The cells were fixed with 2.5% glutaraldehyde for 20 min, dehydrated with a concentration gradient of 75, 85, 95, and 100% ethanol, and then dried. We observed the results using a SEM (Sirion 200, FEI, Hillsboro, OR).

2.8. Micro-computed tomography analysis

Female Sprague–Dawley rats (200–250 g, 6/group) were obtained from the Shanghai Ninth People's Hospital Animal Center Research Committee of Shanghai Ninth People's Hospital (Shanghai, China). Approval documents for all the animal processes were signed by the animal hospital affiliated with Shanghai Jiao Tong University. The surgical plan was as follows. Twenty female rats (200–250 g) were used as animal models. A skull defect model of bilateral critical size was implemented to assess bone regeneration. The height and diameter of the bone defect were 2 mm and 5 mm, accordingly. After the rat was anesthetized, the hair of the skull was removed, the skin was cut, and the fascia was removed. The scaffolds ($n = 10$) were filled in the defect sites, and the scalps were sutured.

Twelve weeks following the surgery, the rats were euthanized by dislocation after an intraperitoneal injection of sodium pentobarbital. After soaking in the solution of 4% phosphate-buffered formalin, the samples were discerned employing a micro-CT system (mCT-80, Scanco Medical AG, Switzerland) with a current of 88 μ A, voltage of 90 kV, and voxel size of 28 μ m. Finally, the 3D image was reconstructed based on CT images.

2.9. Histological analysis

We performed fluorescent double-labeling of the new bone formation

with calcein (30 mg/kg, Sigma–Aldrich) and alizarin red (30 mg/kg, Sigma–Aldrich), which were injected 21 and 3 days before the samples were harvested, accordingly. Cranium samples containing CPS or Fe-CPS bioceramic materials were harvested and soaked in 4% paraformaldehyde for 7 days. We performed fluorescent labeling (alizarin red, 543/580–670 nm; calcein, 488/500–550 nm) observation with a confocal laser scanning microscope (Leica, Heidelberg, Germany) after the undecalcified specimens were inserted in polymethyl methacrylate and sliced into 150-mm-thick sections employing a microtome (Leica, Hamburg, Germany). The mineralization rate was simultaneously quantified. Other specimens were decalcified in 10% ethylenediaminetetraacetic acid for 30 days and subsequently inserted in paraffin. After being sliced to a thickness of 5 μ m, the sections were mounted on polylysine-coated microscope slides. The sections were then stained with hematoxylin and eosin (H&E) or Masson's trichrome. Finally, we performed morphological analysis using optical microscopy.

2.10. Immunohistochemistry for bone morphogenetic protein 2, osteoprotegerin, and type 1 collagen protein

We obtained monoclonal antibodies against bone morphogenetic protein-2 (BMP-2), osteoprotegerin (OPG), and human type I collagen (COL1) from Sigma–Aldrich (Castle Hill, NSW, Australia). The samples were blocked with 0.1% bovine serum albumin using 10% swine serum and allowed to incubate at 4 °C overnight with primary antibodies for BMP-2, OPG, and COL1, which were diluted to 1:200. Finally, we performed morphological analysis by optical microscopy.

3. Results

3.1. Morphology and structure of Fe-CPS

Fig. 1 shows the fracture morphology of porous Fe-CPS scaffolds. The achievements illustrated that with the addition of PEG, most of the pores formed were larger than 150 μ m, which favors cell migration, bone formation, and vascularization [34].

3.2. Phase composition and release of Fe-CPS bioceramics

The patterns of XRD for the Fe-CPS bioceramics (Fig. 2) show that all the diffraction peaks of Fe-CPS bioceramics referred to CPS (PDF# 40–0393), and no evident ferric oxide phase was detected owing to the restriction of XRD detection with the increase in ferric oxide content. Fe-CPS bioceramics were investigated thoroughly for determining their phase composition in our previous work [30], and the results showed that the calcium silicate phase appeared with the addition of ferric oxide. Table 1 shows the calcium, phosphate, silicon, and iron concentrations of MEM- α after immersion. After the immersion of the Fe-CPS bioceramics, the calcium, phosphate, silicon, and iron concentrations in MEM- α changed clearly. With the addition of ferric oxide, the calcium and silicon concentrations in MEM- α decreased, indicating that ferric oxide could inhibit the release of calcium and silicon. With the increase in ferric oxide content, however, there were no significant trends in calcium, phosphate, silicon, and iron concentrations. Moreover, MEM- α immersed in the 1.0Fe-CPS bioceramic solution showed the maximum Fe concentration.

3.3. Cytotoxicity of Fe-CPS bioceramics

We observed the cytotoxicity of the Fe-CPS bioceramic using CCK-8 and SEM images of hBMSC adhesion on the surface. The results of the CCK-8 test demonstrated no significant difference between CPS and each group of Fe-CPS bioceramics, as demonstrated in Fig. 3. The SEM images of hBMSC adhesion on the surface of the CPS and each group of Fe-CPS bioceramics also showed that the cells were spread widely on each material and that the morphologies of the cells were similar, as shown in Fig. 4.

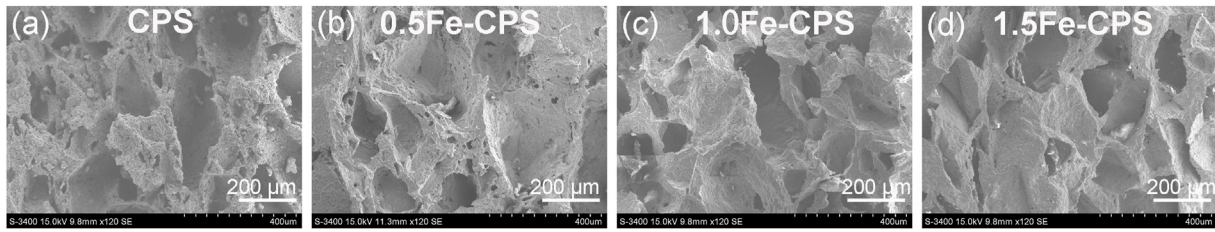


Figure 1. Fracture morphologies of the porous CPS and 0.5, 1.0, 1.5 Fe-CPS scaffolds, respectively.

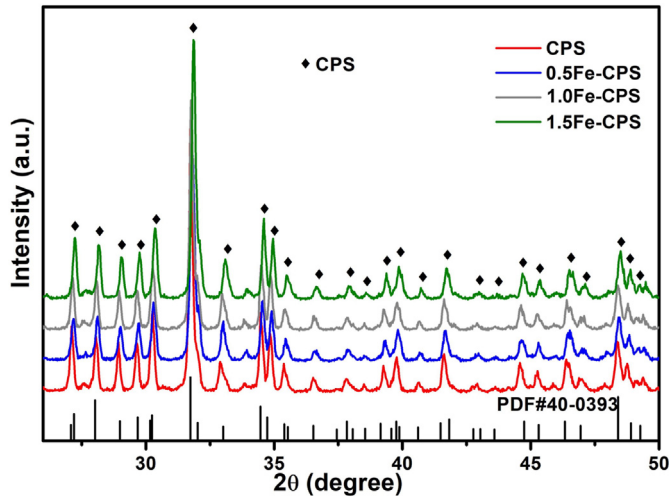


Figure 2. XRD patterns of the Fe-CPS bioceramics.

Table 1

Ion concentrations of the culture medium after immersed with Fe-CPS bioceramics for 24 h.

Name	Ca(μg/mL)	P(μg/mL)	Si(μg/mL)	Fe(μg/mL)
MEM-α	66.27	31.06	4.19	
0Fe-CPS	99.36	22.42	43.49	
0.5Fe-CPS	92.10	22.81	38.20	0.013
1.0Fe-CPS	94.14	31.48	26.61	0.063
1.5Fe-CPS	94.32	27.60	32.23	0.033

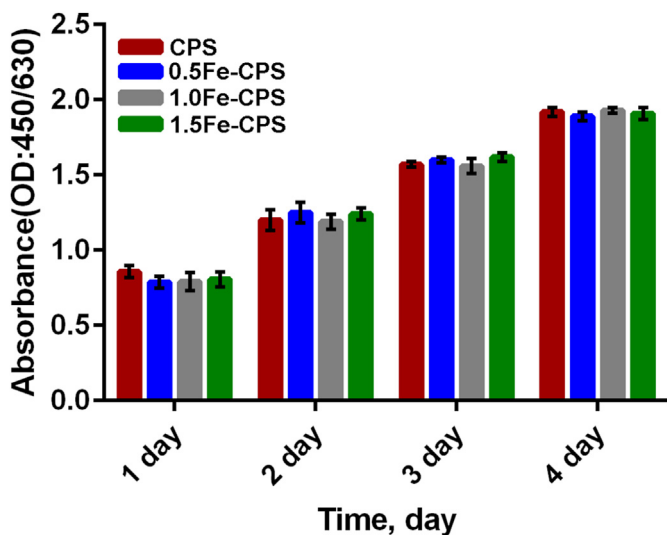


Figure 3. Results of the CCK-8 test for Fe-CPS bioceramics with different iron addition.

3.4. Immunofluorescence of adhesion-related proteins on Fe-CPS bioceramics *in vitro*

To investigate the expression of adhesion-related proteins in the early stage of cell adhesion after culturing on Fe-CPS bioceramics, immunofluorescence staining of the adhesion-related proteins, including rho-protein, vinculin, and myosin, was performed. The extract of the scaffold materials (CPS, 0.5Fe-CPS, 1.0Fe-CPS, and 1.5Fe-CPS) was used to culture 3T3-E1 cells for 24 h. The cells of each group were rinsed three times with PBS for 10 min each time. Next, the cells were fixed with 4% paraformaldehyde for 10 min. PBS was used to wash the cells thrice following which they were allowed to incubate with the primary antibody at 4 °C overnight. Finally, each group was incubated with a fluorescent secondary antibody for 2 h. An LSM5 confocal microscope (Carl Zeiss AG) was employed for observing the fluorescence intensity. The results showed that the fluorescence intensity of the cells co-cultured with Fe-CPS was substantially superior to that of the pure CPS group, indicating that Fe-CPS bioceramics could promote the adhesion of hBMSCs. The 1.0Fe-CPS group once again showed the most obvious result, as shown in Fig. 5.

3.5. Osteogenic potential of Fe-CPS bioceramics *in vitro*

The effect of Fe-CPS bioceramics on osteogenesis *in vitro* by ALP and alizarin staining and PCR for the ALP, OPN, and RUNX2 genes. After culturing for 7 days, ALP staining results showed that all groups presented good ALP activity and the ALP activity of Fe-CPS bioceramics was substantially superior to that of pure CPS, especially for the 1.0Fe-CPS group, as shown in Fig. 6A. The results of Alizarin staining demonstrated that the number of mineralization nodules on the surface of each Fe-CPS group was greater than that of the CPS. Once again, the 1.0Fe-CPS group showed the maximum number of mineralization nodules, as shown in Fig. 6B. We further evaluated the positive effect of Fe-CPS bioceramic on osteogenesis by RT-PCR for ALP, OPN, and RUNX2, which represent osteoblast differentiation. The outcome revealed that the extent of expression of these genes were significantly different among the CPS and Fe-CPS groups, and the expression level for the 1.0Fe-CPS group was almost 1.5 times higher in comparison to that of the other two Fe-CPS groups, as shown in Fig. 7.

3.6. Osteogenic activity of Fe-CPS bioceramics *in vivo*

We investigated the new bone formation capability of Fe-CPS bioceramics *in vivo* using the micro-CT test, fluorescent double-labeling of alizarin red and calcein, HE, and Masson staining. We also investigated the effect of Fe-CPS bioceramics on osteogenesis through immunohistochemical analysis of BMP-2, OPG, and COL1, which represented osteoblast differentiation.

The 3D model reconstruction based on micro-CT images manifested a clear increase in new bone formation around the bioceramics in the 1.0Fe-CPS group at 12 weeks, as shown in Fig. 8A. Quantitative analysis revealed that the bone volume/total volume ratio of the Fe-CPS groups was 3–5 times greater than that of the CPS group, and the ratio for the 1.0Fe-CPS group was considerably higher in comparison to that of the

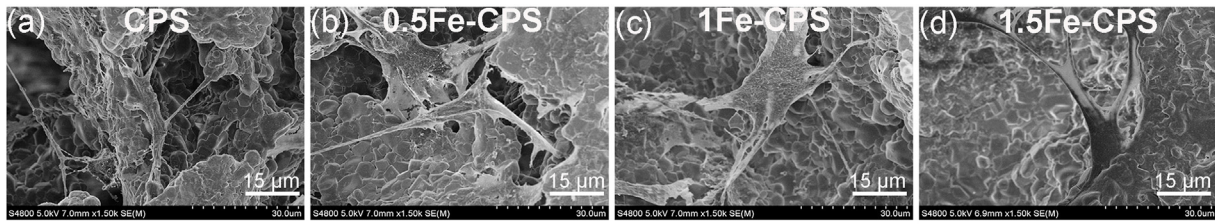


Figure 4. SEM images of hBMSC adhesion on the surface of CPS and each group of Fe-CPS showed that the cells spread well on each material and the cell morphologies were similar.

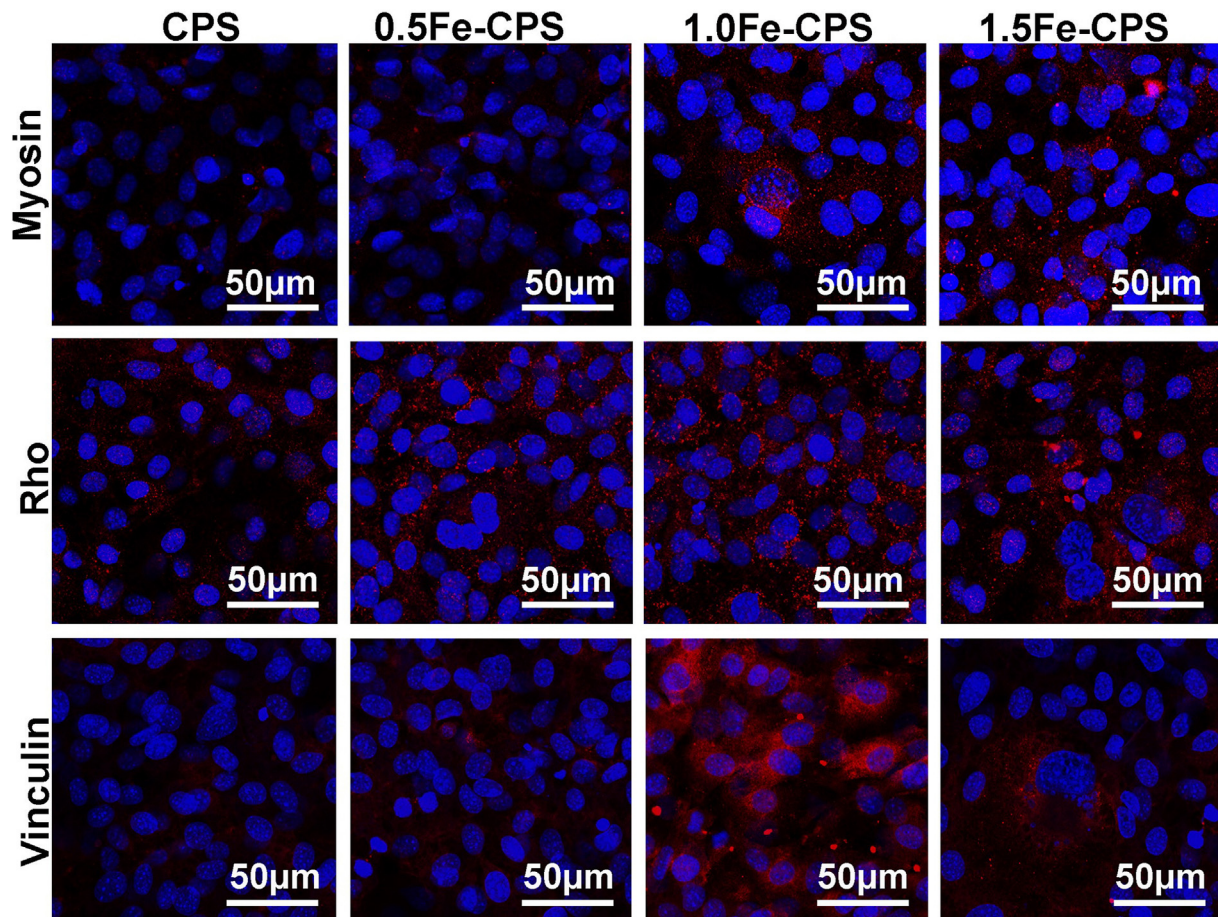


Figure 5. Results of immunofluorescence of the adhesion-related proteins Rho-protein, vinculin, and myosin. These proteins combined with certain antibodies showed red under laser scanning confocal microscope.

other two Fe-CPS groups. The bone mineral density of the 0.5Fe-CPS and 1.5Fe-CPS groups was superior to that of the CPS group, but the discrepancy was not statistically meaningful. However, the bone mineral density of the 1.0Fe-CPS group was substantially superior to that of the other groups, as shown in Fig. 8C. These results revealed that the volume of new bone formed in 1.0Fe-CPS mice was obviously faster than in other groups, and Fe at certain concentrations in this group may have an evident effect on new bone formation ability increasing to CPS.

The results of the fluorescent double-labeling were similar to those of micro-CT. The fluorescent double-labeling images showed improved new bone formation for Fe-CPS; however, the quantitative analysis showed that the CPS group and the 0.5Fe-CPS and 1.5Fe-CPS groups were not significantly different. In addition, the mineralization rate for the 1.0Fe-CPS group was considerably higher in comparison to that of the other groups. The mineralization rate for the 1.0Fe-CPS group was greater than 2.5 times greater than that of the CPS group, as shown in Fig. 8 B/C. The

new bone morphology observed by HE and Masson staining demonstrated improved new bone formation in the surrounding area of the Fe-CPS bioceramics and in the materials, with the most obvious improvement in the 1.0Fe-CPS group, as shown in Fig. 9. Compared with the immunohistochemical analysis, both the images and the quantitative analysis showed significantly higher expression of osteoblast differentiation associated with BMP-2, OPG, and COL1, which were similar to previous results. The most notable difference was again seen in the 1.0Fe-CPS group, as shown in Fig. 10.

4. Discussion

Previous studies have shown that Fe is critical for bone metabolism and that the lack of Fe can affect bone formation. Fe can affect collagen synthesis, vitamin D metabolism, and maturation, which are critical for bone formation [28]. Medeiros et al. observed significant reductions in

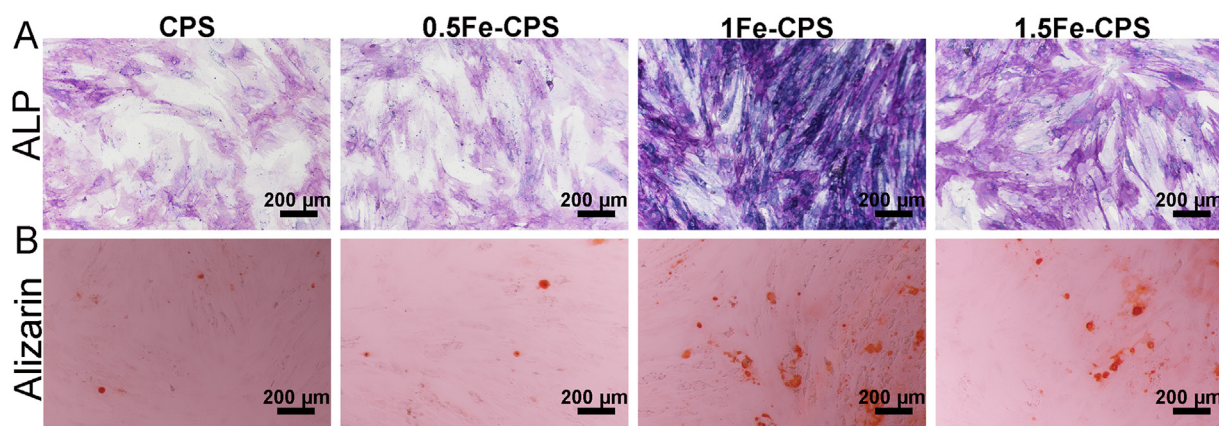


Figure 6. ALP and alizarin staining results showed higher ALP activity and larger numbers of mineralization nodules on the surface of each Fe-CPS group, especially for the 1.0Fe-CPS group.

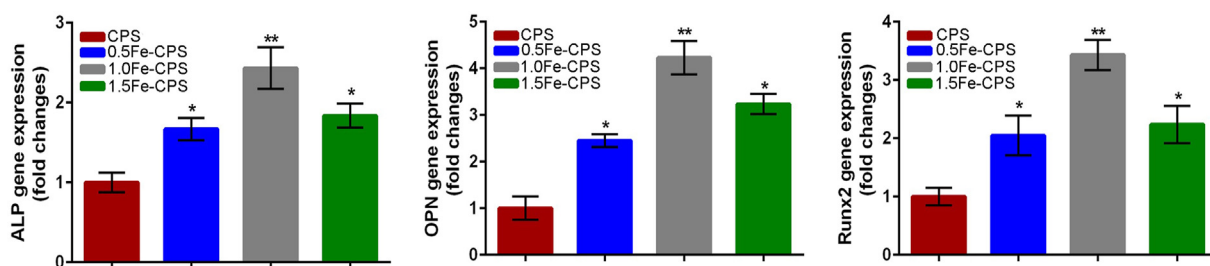


Figure 7. PCR results for the ALP, OPN, and RUNX2 genes expression showed higher expression level in Fe-CPS groups and highest in 1.0Fe-CPS (* and ** represent different significance of $P < 0.05$, 0.01 , 0.001 , respectively).

bone density and reduced cortical bone area in rats with dietary iron deficiency [35]. Recent studies have also reported that appropriate amounts of Fe added to biomaterials are safe and clearly promote biomaterial bioactivity [18,31–33]. Fe is therefore a promising element that is expected to improve the osteoinductivity of artificial bone repair biomaterials. Therefore, we added Fe in the form of Fe_2O_3 to CPS and investigated the osteogenic activity and new bone formation ability of Fe-CPS bioceramics. In addition, we analyzed the amount of Fe_2O_3 added to CPS.

The cytotoxicity test of Fe in the Fe-CPS bioceramic showed no considerable difference between the Fe-CPS and CPS groups in the CCK-8 result. The SEM images showed good hBMSC adhesion and spread on the surface of the Fe-CPS ceramics. We can therefore conclude that CPS with 0.5%, 1.0%, or 1.5% Fe_2O_3 has sufficient biocompatibility, which is in line with previous reports. Vahabzadeh et al. reported adding Fe_2O_3 to β -tricalcium phosphate and showed that up to 1.0 wt% Fe_2O_3 in β -tricalcium phosphate had good biocompatibility [18]. Gupta et al. detected cell responses to iron-containing materials, with results showing good biocompatibility [36]. Zhang et al. reported that Fe toxicity depends on the Fe^{3+} concentration; the authors cultured mBMSCs using 1/1, 1/4, 1/16, 1/64, 1/128, and 1/256 iron extracts and the same series of pc-extract. They observed a slight cytotoxic effect on mBMSCs at higher Fe^{3+} concentrations in the 1/1 and 1/4 iron-extract and pc-extract groups in the proliferation test and images of the live/dead assay. The authors documented that Fe^{3+} enhanced the proliferation of mBMSCs on day 7, in cases when the Fe^{3+} concentrations were low. In the lower concentration groups, the live/dead assay revealed good mBMSC viability [33]. This indicated that excess Fe could cause side effects on mBMSCs, and the iron content in our Fe-CPS ceramics was under the safe line.

In our study, the addition of Fe_2O_3 to CPS promoted the osteogenic activity of the ceramics *in vitro*. The ALP staining results showed that the ALP activity of the Fe-CPS bioceramics was notably high in comparison to that of the CPS, especially for the 1.0Fe-CPS group. The expression of

osteogenic differentiation-related genes was observed to be considerably different between the CPS and Fe-CPS groups as demonstrated by the results of RT-PCR. The 1.0Fe-CPS group exhibited an evidently higher degree of expression than that of the other two Fe-CPS groups. This indicated that Fe could promote osteoblast differentiation by upregulating osteogenic markers, such as ALP, OPN, and RUNX2. Alizarin staining results showed more mineralization nodules on the surface of each Fe-CPS group, revealing that mineralization of the osteoblasts' extracellular matrix was also increased by adding Fe to CPS.

It has previously been reported that the bioactivity effects were associated with the amount of Fe_2O_3 added to CPS, and within limits, larger quantities of Fe showed greater promoting effects. However, when a certain limit is reached, excess Fe has the opposite effect on osteoblast differentiation compared to a more suitable amount of Fe [33]. Interestingly, the inductively coupled plasma test in our study showed greater Fe ion release in the 1.0Fe-CPS group, an unexpected result given that we expected greater Fe ion release by the 1.5Fe-CPS group. The reason for this finding remains unclear. The test was repeated three times, and each time the result showed that the inflection point of Fe release occurred in the 1.0Fe-CPS group. This result agreed with the results of the bioceramics' *in vitro* inductivity test. A possible explanation could be that our Fe ion concentration was in the safe range and that appropriate amounts of Fe ions can have a positive effect on osteoblast differentiation and prevent the adverse effects of Fe deficiency. Vahabzadeh et al. showed that Fe added to TCP can promote *in vitro* osteoblast cellular interactions in TCP ceramics [18]. Zhang et al. also reported that Fe improves the osteoinductivity of calcium phosphate cement [33]. As previously mentioned, Fe deficiency can have negative effects on bone formation [35]. Katsumata et al. reported that a lack of dietary Fe can lead to significantly reduced bone formation rates and osteoclast surfaces in the lumbar vertebrae [27]. Another study by same researchers shows that in the dietary Fe deficiency group, serum osteocalcin concentrations, bone mineral density, bone mineral content, and femur mechanical

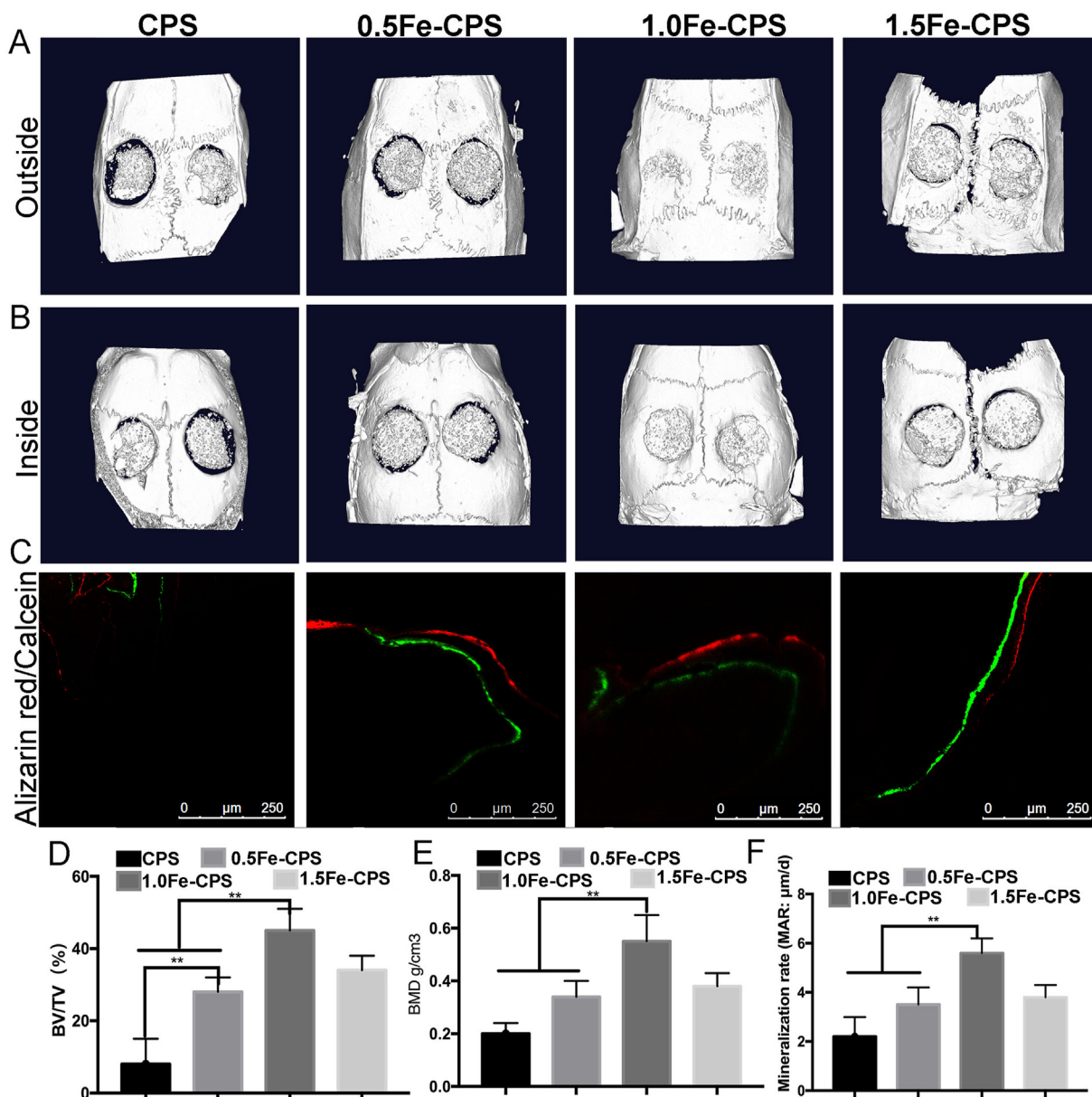


Figure 8. Micro-CT results of the *in vivo* samples. A. The 3D model reconstruction based on micro-CT images demonstrated a clear increase in new bone formation around the bioceramics in the 1.0Fe-CPS group. B & C. The mineralization rate for the 1.0Fe-CPS group was considerably greater in comparison to that of other groups. C. The bone mineral density of the 1.0Fe-CPS group was considerably greater than that of the other groups. D. New bone volume/tissue volume (BV/TV), E. Local bone mineral density (BMD) analysis and F. Mineralization rate (* and** represent different significance of P < 0.05, 0.01,0.001, respectively) .

strength were all considerably lower. Fe deficiency can also cause new bone development to be disrupted, as suggested by Katsumata et al. [26].

The immunofluorescence images of the adhesion-related proteins, Rho-protein, vinculin, and myosin showed that the fluorescence intensity of the cells co-cultured with Fe-CPS was substantially higher than that of CPS. The 1.0Fe-CPS group once again showed the most obvious results. Therefore, we assumed that the addition of Fe created a more favorable surface for cell adhesion. Ghezzi et al. reported that the material surface could affect the protein adsorption pattern of the material, thereby promoting cell adhesion and osteoblast differentiation [37]. In their study, the protein vinculin in cells showing better adhesion was more homogeneously distributed. We also found a higher immunofluorescence intensity for vinculin in the Fe-CPS group. Przekora et al. and other researchers also found that the surface properties of biomaterials could influence protein adsorption and further affect osteoblast adhesion [38–41]. Robust cell adhesion is necessary to promote the cell

colonization of biomaterials and differentiation of progenitors [37], which might be an important Fe pathway in CPS for promoting *in vitro* osteoblast differentiation.

As for the *in vivo* test for the ceramics' new bone formation ability, the 3D model reconstructed from micro-CT images and the morphology observation using HE staining showed more satisfactory new bone formation in the Fe-CPS groups, both in the connection area between the ceramics and the host bone and in the ceramics. The quantitative analysis based on the micro-CT images showed that the bone volume/total volume ratios of the Fe-CPS groups were 3–5 times higher in comparison to that of the CPS group, and the fluorescent double-labeling images showed the largest width between the two labels, confirming that the Fe-CPS ceramics had superior new bone formation ability. Consistent with the *in vitro* test results, the most obvious promoting effects were observed in the 1.0Fe-CPS group. Masson staining showed that the Fe-CPS groups had synthesized more collagen, which is rich in bone tissue, a result that

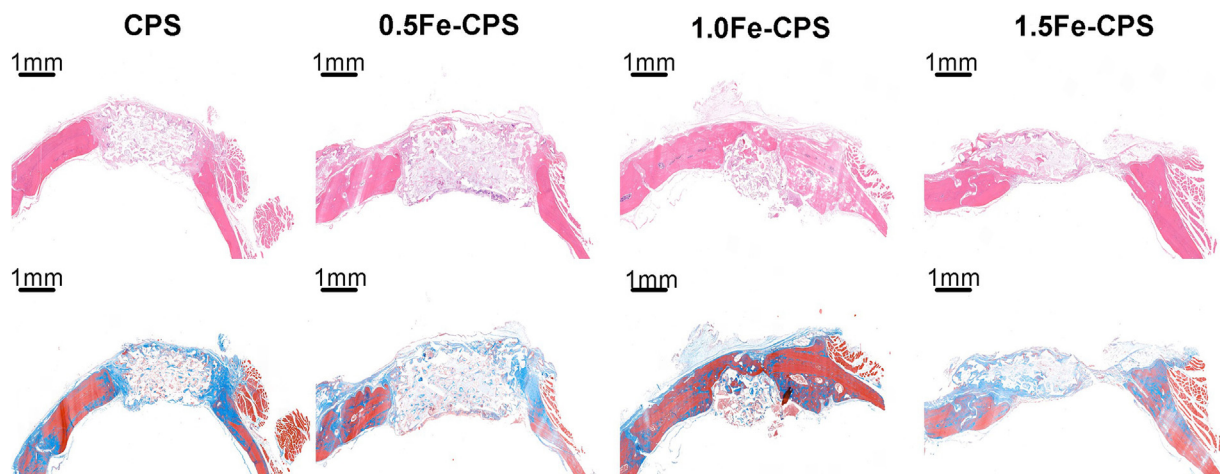


Figure 9. Outcomes of HE and Masson staining exhibited improved formation of new bones in the surrounding area of the Fe-CPS bioceramics and in the central area of the materials, with the most obvious improvement in the 1.0Fe-CPS group.

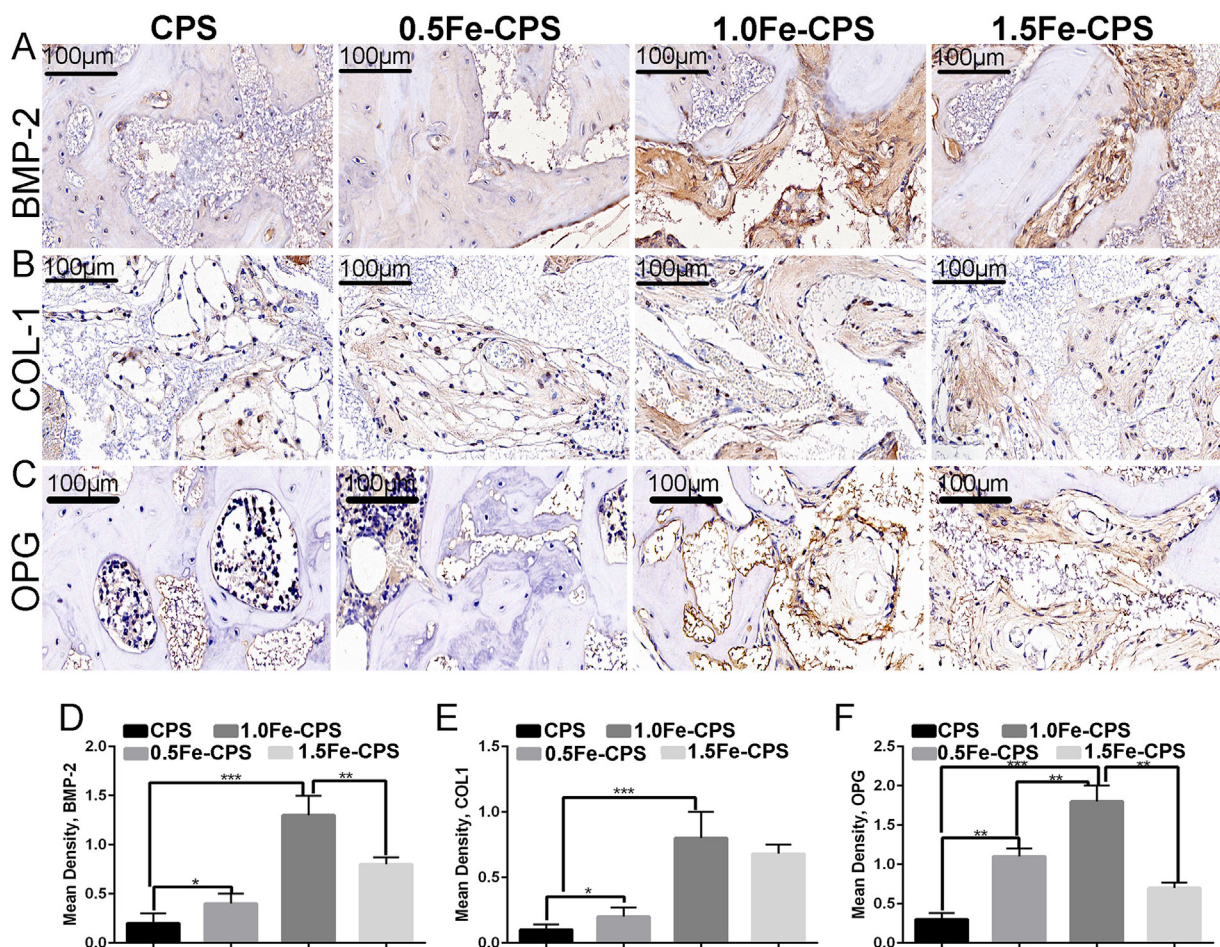


Figure 10. Images and quantitative analyzes of immunohistochemical results showed significantly higher expression of osteoblast differentiation associated with BMP-2 (A&D), COL1 (B&E), OPG (C&F) in Fe-CPS groups. The most significant difference was once again seen in the 1.0Fe-CPS group. (* , ** , *** represent different significance of $P < 0.05$, 0.01 , 0.001 , respectively).

could be due to greater new bone formation, given that Fe is critically involved in collagen production [23].

The immunohistochemical analysis, imaging, and quantitative analysis showed significantly higher expression of osteoblast differentiation associated with BMP-2, OPG, and COL1; the 1.0Fe-CPS group showed the most significant results, revealing that osteoblast differentiation in the

Fe-CPS groups was more active than in the CPS group. Therefore, we can assume that promoting osteoblast differentiation is one of the factors that Fe added to CPS improves new bone formation in rats.

5. Conclusion

In this study, we looked into the effects of Fe₂O₃ addition on the osteogenic activity and new bone formation ability of CPS ceramics. The outcomes imply that the addition of Fe₂O₃ to CPS had no adverse effects on the proliferation and adhesion of MC3T3-E1 cells, while it could obviously enhance osteoblast differentiation. Moreover, Fe-CPS bioceramics showed greater activated osteogenic differentiation and enhanced new bone formation *in vivo*. The study also revealed that the most suitable Fe₂O₃ content in CPS was 1.0 wt%.

Therefore, it can be concluded that adding Fe₂O₃ to CPS can not only improve the bending strength of the ceramics but also promote osteogenic activity and new bone formation ability. Owing to their excellent new bone formation abilities and good mechanical strengths, Fe-CPS bioceramics exhibit great potential for application as materials for bone tissue engineering.

Acknowledgments

This study was sponsored by the National Nature Science Foundation of China (Grant Nos. 31900941 and 82002270) and the Interdisciplinary Program of Shanghai Jiao Tong University (Project No. ZH2018QNA06).

References

- Meng X, Ziadlou R, Grad S, Alini M, Wen C, Lai Y, et al. Animal models of osteochondral defect for testing biomaterials. *Biochem Res Int* 2020;2020:9659412.
- Sargolzaei-Aval F, Saberi EA, Arab MR, Sargolzaei N, Zare E, Shahraki H, et al. Reconstruction of mandibular defects using synthetic octacalcium phosphate combined with bone matrix gelatin in rat model. *Dent Res J* 2020;17(1):10–8.
- Sparks DS, Saifzadeh S, Savi FM, Dlaska CE, Berner A, Henkel J, et al. A preclinical large-animal model for the assessment of critical-size load-bearing bone defect reconstruction. *Nat Protoc* 2020;15(3):877–924.
- Zhang C, Zhu C, Yu G, Deng K, Yu L. Management of infected bone defects of the lower extremities by three-stage induced membrane technique. *Med Sci Mon Int Med J Exp Clin Res* 2020;26:e919925.
- Baldwin P, Li DJ, Austin DA, Mir HS, Yoon RS, Koval KJ. Autograft, allograft, and bone graft substitutes: clinical evidence and indications for use in the setting of orthopaedic trauma surgery. *J Orthop Trauma* 2019;33(4):203–13.
- García-Gareta E, Coathup MJ, Blunn GW. Osteoinduction of bone grafting materials for bone repair and regeneration. *Bone* 2015;81:112–21.
- Nau C, Simon S, Schaible A, Seebach C, Schröder K, Marzi I, et al. Influence of the induced membrane filled with syngeneic bone and regenerative cells on bone healing in a critical size defect model of the rat's femur. *Injury* 2018;49(10):1721–31.
- Oryan A, Alidadi S, Moshiri A, Maffulli N. Bone regenerative medicine: classic options, novel strategies, and future directions. *J Orthop Surg Res* 2014;9(1):18.
- Yang P, Xing J, Liu J, Luo F, Wu X, Yu B, et al. Individual tissue-engineered bone in repairing bone defects: a 10-year follow-up study. *Tissue Eng* 2020;26(15–16):896–904.
- Lu W, Duan W, Guo Y, Ning C. Mechanical properties and *in vitro* bioactivity of Ca₅(PO₄)₂SiO₄ bioceramic. *J Biomater Appl* 2012;26(6):637–50.
- Duan W, Ning C, Tang T. Cytocompatibility and osteogenic activity of a novel calcium phosphate silicate bioceramic: Silicocarnotite. *J Biomed Mater Res* 2013;101(7):1955–61.
- Gotz W, Tobiasch E, Witzleben S, Schulze M. Effects of silicon compounds on biomineralization, osteogenesis, and hard tissue formation. *Pharmaceutics* 2019;11(3).
- Mao L, Xia L, Chang J, Liu J, Jiang L, Wu C, et al. The synergistic effects of Sr and Si bioactive ions on osteogenesis, osteoclastogenesis and angiogenesis for osteoporotic bone regeneration. *Acta Biomater* 2017;61:217–32.
- Chen Y, Kawazoe N, Chen G. Preparation of dexamethasone-loaded biphasic calcium phosphate nanoparticles/collagen porous composite scaffolds for bone tissue engineering. *Acta Biomater* 2018;67:341–53.
- Kim JA, Lim J, Naren R, Yun HS, Park EK. Effect of the biodegradation rate controlled by pore structures in magnesium phosphate ceramic scaffolds on bone tissue regeneration *in vivo*. *Acta Biomater* 2016;44:155–67.
- Samavedi S, Whittington AR, Goldstein AS. Calcium phosphate ceramics in bone tissue engineering: a review of properties and their influence on cell behavior. *Acta Biomater* 2013;9(9):8037–45.
- Stastny P, Sedlacek R, Suchy T, Lukasova V, Rampichova M, Trunec M. Structure degradation and strength changes of sintered calcium phosphate bone scaffolds with different phase structures during simulated biodegradation *in vitro*. *Mater Sci Eng C Mater Biol Appl* 2019;100:544–53.
- Vahabzadeh S, Bose S. Effects of iron on physical and mechanical properties, and osteoblast cell interaction in β -tricalcium phosphate. *Ann Biomed Eng* 2017;45(3):819–28.
- Bracci B, Torricelli P, Panzavolta S, Boanini E, Giardino R, Bigi A. Effect of Mg(2+), Sr(2+), and Mn(2+) on the chemico-physical and *in vitro* biological properties of calcium phosphate biomimetic coatings. *J Inorg Biochem* 2009;103(12):1666–74.
- Fielding G, Bose S. SiO₂ and ZnO dopants in three-dimensionally printed tricalcium phosphate bone tissue engineering scaffolds enhance osteogenesis and angiogenesis *in vivo*. *Acta Biomater* 2013;9(11):9137–48.
- Tarafder S, Davies NM, Bandyopadhyay A, Bose S. 3D printed tricalcium phosphate scaffolds: effect of SrO and MgO doping on *in vivo* osteogenesis in a rat distal femoral defect model. *Biomater Sci* 2013;1(12):1250–9.
- Tarafder S, Dornell WS, Bandyopadhyay A, Bose S. SrO- and MgO-doped microwave sintered 3D printed tricalcium phosphate scaffolds: mechanical properties and *in vivo* osteogenesis in a rabbit model. *J Biomed Mater Res B Appl Biomater* 2015;103(3):679–90.
- Balogh E, Paragh G, Jeney V. Influence of iron on bone homeostasis. *Pharmaceutics* 2018;11(4).
- Montufar EB, Casas-Luna M, Horynova M, Tkachenko S, Fohlerova Z, Diaz-de-la-Torre S, et al. High strength, biodegradable and cytocompatible alpha tricalcium phosphate-iron composites for temporal reduction of bone fractures. *Acta Biomater* 2018.
- Vahabzadeh S, Bose S. Effects of iron on physical and mechanical properties, and osteoblast cell interaction in beta-tricalcium phosphate. *Ann Biomed Eng* 2017;45(3):819–28.
- Katsumata S, Tsuboi R, Uehara M, Suzuki K. Dietary iron deficiency decreases serum osteocalcin concentration and bone mineral density in rats. *Biosci Biotechnol Biochem* 2006;70(10):2547–50.
- Katsumata S, Katsumata-Tsuboi R, Uehara M, Suzuki K. Severe iron deficiency decreases both bone formation and bone resorption in rats. *J Nutr* 2009;139(2):238–43.
- McGillivray G, Skull SA, Davie G, Kofoed SE, Frydenberg A, Rice J, et al. High prevalence of asymptomatic vitamin D and iron deficiency in East African immigrant children and adolescents living in a temperate climate. *Arch Dis Child* 2007;92(12):1088–93.
- Zhang D, Wong CS, Wen C, Li Y. Cellular responses of osteoblast-like cells to 17 elemental metals. *J Biomed Mater Res* 2017;105(1):148–58.
- Deng F, Rao J, Ning C. Ferric oxide: a favorable additive to balance mechanical strength and biological activity of silicocarnotite bioceramic. *J Mech Behav Biomed Mater* 2020;109:103819.
- Tkachenko S, Horynová M, Casas-Luna M, Diaz-de-la-Torre S, Dvořák K, Celko L, et al. Strength and fracture mechanism of iron reinforced tricalcium phosphate cement fabricated by spark plasma sintering. *J Mech Behav Biomed Mater* 2018;81:16–25.
- Tran N, Hall D, Webster TJ. Mechanisms of enhanced osteoblast gene expression in the presence of hydroxyapatite coated iron oxide magnetic nanoparticles. *Nanotechnology* 2012;23(45):455104.
- Zhang J, Shi HS, Liu JQ, Yu T, Shen ZH, Ye JD. Good hydration and cell-biological performances of superparamagnetic calcium phosphate cement with concentration-dependent osteogenesis and angiogenesis induced by ferric iron. *J Mater Chem B* 2015;3(45):8782–95.
- Li X, van Blitterswijk CA, Feng Q, Cui F, Watari F. The effect of calcium phosphate microstructure on bone-related cells *in vitro*. *Biomaterials* 2008;29(23):3306–16.
- Medeiros DM, Plattner A, Jennings D, Stoecker B. Bone morphology, strength and density are compromised in iron-deficient rats and exacerbated by calcium restriction. *J Nutr* 2002;132(10):3135–41.
- Gupta AK, Gupta M. Synthesis and surface engineering of iron oxide nanoparticles for biomedical applications. *Biomaterials* 2005;26(18):3995–4021.
- Ghezzi B, Lagonegro P, Pece R, Parisi L, Bianchi M, Tatti R, et al. Osteoblast adhesion and response mediated by terminal -SH group charge surface of SiOx/Cy nanowires. *J Mater Sci Mater Med* 2019;30(4):43.
- Lin M, Wang H, Ruan C, Xing J, Wang J, Li Y, et al. Adsorption force of fibronectin on various surface chemistries and its vital role in osteoblast adhesion. *Biomacromolecules* 2015;16(3):973–84.
- Mavropoulos E, Hausen M, Costa AM, Alves G, Mello A, Ospina CA, et al. The impact of the RGD peptide on osteoblast adhesion and spreading on zinc-substituted hydroxyapatite surface. *J Mater Sci Mater Med* 2013;24(5):1271–83.
- Przekora A, Benko A, Blazewicz M, Ginalska G. Hybrid chitosan/ β -1,3-glucan matrix of bone scaffold enhances osteoblast adhesion, spreading and proliferation via promotion of serum protein adsorption. *Biomed Mater* 2016;11(4):045001.
- Webster TJ, Ergun C, Doremus RH, Bizios R. Hydroxylapatite with substituted magnesium, zinc, cadmium, and yttrium. II. Mechanisms of osteoblast adhesion. *J Biomed Mater Res* 2002;59(2):312–7.